Defects in Irradiated Silicon: Electron Paramagnetic Resonance and Electron-Nuclear Double Resonance of the Si-E Center

G. D. WATKINS AND J. W. CORBETT
General Electric Research Laboratory, Schenectady, New York
(Received 7 January 1964)

The Si-E center is one of the dominant defects produced by electron irradiation in phosphorus-doped vacuum floating zone silicon. It introduces an acceptor level at $\sim(E_c-0.4)$eV and gives rise to an electron paramagnetic resonance when this level does not contain an electron. As a result of electron paramagnetic resonance (EPR) and electron-nuclear double resonance (ENDOR) studies described in this paper, we conclude that the defect is a lattice vacancy trapped next to a substitutional phosphorus atom, with EPR arising from the neutral charge state. The observed hyperfine interactions with P^{31} and neighboring Si^{29} nuclei, as well as the observed g-tensor anisotropy, are discussed in terms of a simple linear combination of atomic orbitals (LCAO) molecular orbital treatment. In addition to the anisotropy associated with the phosphorus-vacancy direction in the lattice, an additional distortion of the defect occurs which is identified in the LCAO treatment as a manifestation of the Jahn-Teller effect. Thermally activated reorientation from one Jahn-Teller distortion to another causes motional broadening and narrowing effects upon the EPR spectrum in the temperature region 60–150°K. The motion is also studied by stress-induced alignment at lower temperatures and the activation energy for this process is determined to be $\sim$0.06 eV. Alignment of the phosphorus-vacancy direction in the lattice is also achieved by stressing at elevated temperatures. The activation energy for this motion is 0.93 ± 0.05 eV. The magnitude and sense of the alignment in both kinds of stress experiments are consistent with the microscopic model of the defect. The role of the phosphorus-vacancy interaction in the diffusion of phosphorus in unirradiated silicon is discussed. Using the published value for the diffusion activation energy for phosphorus in silicon, we estimate the appropriate value for silicon self-diffusion to be 3.94 ± 0.33 eV and the formation energy for the lattice vacancy in silicon to be 3.6 ± 0.5 eV. These are quantities for which no direct experimental values are available. Also included is an appendix which gives estimates of $|\psi_{3s}(0)|^2$ and $\langle r_{3p}^{-3}\rangle$ for the $3p$ atoms aluminum through chlorine.

I. INTRODUCTION

THIS is the third[1] in a series giving detailed descriptions of defects produced by irradiation in silicon. In this paper, we describe electron paramagnetic resonance (EPR) studies of the Si-E center.[2] This center has been discussed briefly in previous publications[3,4] where it was tentatively identified as a phosphorus-vacancy pair. In this paper the arguments leading to this identification are presented, and a model of the microscopic configuration of the defect as well as its electronic structure is presented. Such physical properties as its activation energy for diffusion, its binding energy, etc., are estimated.

Also discussed is the role that this defect plays in the high-temperature diffusion of phosphorus in unirradiated material. From some of the properties of the E center deduced here, we can estimate the activation energy for self-diffusion in silicon as well as the formation energy for the lattice vacancy, quantities for which no direct experimental values are available.

II. EXPERIMENTAL PROCEDURE

The silicon samples[5] studied were n type (phosphorus $\approx10^{15}-10^{16}/cm^{-3}$) which had been grown in vacuum by the floating zone technique. The samples were approximately 0.1 in.$\times$0.1 in.$\times$0.5 in. and were irradiated equally on opposite sides at room temperature by 1.5 MeV electrons from a resonant transformer accelerator. The bombardment current was ≈2.5 $\mu A/cm^2$, the maximum temperature rise in the sample being about 25°C.

The samples were mounted with their long dimension along the axis of a TE_{011} microwave cavity and EPR was studied using a balanced bolometer spectrometer at 20 kMc/sec. Magnetic field modulation and lock-in detection at 94 cps were employed. Most measurements were made in dispersion. At $\leq$20°K, relaxation times are long and rapid passage effects[6] gave absorption-like spectra, 180 deg out of phase with respect to the modulation. Studies at higher temperatures gave the usual derivative of dispersion curves.

For electron-nuclear double resonance (ENDOR)[7] studies, a single turn coil on the end of a coaxial line was introduced into the resonance cavity, as shown in Fig. 1, the open loop at the bottom of the coil allowing it to slip over the previously mounted sample. The coil was driven by a General Radio 1211B Unit Oscillator

[1] The first two are (I) G. D. Watkins and J. W. Corbett, Phys. Rev. **121**, 1001 (1961) and (II) J. W. Corbett, G. D. Watkins, R. S. MacDonald, and R. M. Chrenko, *ibid.* **121**, 1015 (1961). In the remainder of this article they will be referred to as (I) and (II), respectively.

[2] In the remainder of the paper, the prefix "Si-" will be dropped for convenience.

[3] G. D. Watkins, J. W. Corbett, and R. M. Walker, J. Appl. Phys. **30**, 1198 (1959).

[4] G. D. Watkins and J. W. Corbett, Discussions Faraday Soc. **31**, 86 (1961).

[5] Procured from Merck Chemical Company.

[6] A. M. Portis, Phys. Rev. **100**, 1219 (1955), Technical Note No. 1, Sarah Mellon Scientific Radiation Laboratory, University of Pittsburgh, November, 1955 (unpublished); M. Weger, Bell System Tech. J. **39**, 1013 (1960).

[7] G. Feher, Phys. Rev. **103**, 834 (1956).

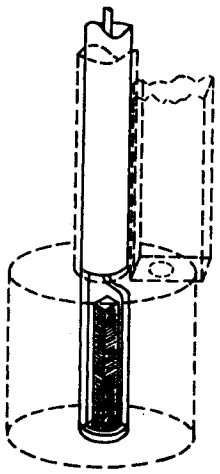

FIG. 1. Single-turn coil assembly introduced into the microwave cavity for ENDOR studies.

and supplied the radio-frequency magnetic field necessary for the nuclear transitions. ENDOR studies were made at 4.2°K by observing a strongly saturated electronic transition in dispersion under normal conditions of magnetic field modulation. The nuclear transition frequencies were detected as a transient change in the electron resonance signal as the radio-frequency oscillator was swept through the nuclear resonance frequency.

The method for applying uniaxial stress to the crystal has been previously described in (I). Briefly, a simple lever and weights outside the cryostat supplies a force to a stainless-steel rod (inserted into the entry tube in place of the ENDOR coaxial line) which in turn transmits this force directly to the end of the crystal, thus compressing it along its long dimension.

Studies versus temperature were made below 77°K by first cooling to 20°K, expelling the liquid H_2 coolant, and observing as the cavity plus crystal warmed up to the 77°K of the cryostat heat shield. For higher temperatures, a heater connected to the wave guide approximately 6 in. above the cavity was used. Temperature was monitored by a copper-constantan thermocouple on the cavity.

III. GENERAL RESULTS AND DISCUSSION

A. Experimental Results

1. Summary of Previous Work

Previous studies[3] have shown the following:

(a) The E center is the dominant spin-resonance center produced in phosphorus-doped *vacuum floating zone* silicon by 1.5 MeV electron irradiation at room temperature. It does not appear in the initial stages of the irradiation but only after the Fermi level has receded to $\approx(E_c-0.4)$eV as a result of the irradiation. The E center is thus associated with a net acceptor level at $\approx(E_c-0.4)$eV[8] and *is observed only when this level does not contain an electron.*

[8] We found this level to be at 0.43 eV. Other investigators have reported the dominant acceptor level in phosphorus-doped floating zone silicon to be at (i) 0.38 eV [G. K. Wertheim and D. E. Buchanan, J. Appl. Phys. **30**, 1232 (1959)], (ii) 0.4 eV [H. Saito, M. Hirata, and T. Horiuchi, J. Phys. Soc. Japan **10**, Suppl. III, 246 (1963)], and (iii) 0.47 eV [E. Sonder and L. C. Templeton, J. Appl. Phys. **34**, 3295 (1963)]. These discrepancies may reflect the presence of other defects with energies near to that of the E center (see Ref. 4).

(b) Hyperfine interaction with 4.7% abundant Si^{29} has shown that the E-center resonance arises from an unpaired electron that is highly localized on one silicon atom. An additional hyperfine interaction with an impurity atom with a 100% abundant nuclear isotope of $I=\frac{1}{2}$ is also observed. This was suggested to be due to a neighboring phosphorus atom.

(c) The E center has not been observed in *pulled* n-type silicon (containing oxygen $\approx10^{18}$ cm^{-3}). Instead in this material the dominant defect observed is the Si-A center,[1] which we have identified as a substitutional oxygen atom, presumably formed when a mobile lattice vacancy is trapped by an interstitial oxygen impurity. This reciprocal behavior between Si-A and Si-E centers, depending upon the concentration of oxygen, led us to suggest that the E center also results from a trapped vacancy, in this case trapped by a phosphorus atom.

2. EPR Spectrum

Figure 2 shows a recording of the E-center spectrum. There is a strong central group made up of doublets and, at higher gain, satellites are observed showing the same doublet structure. Figure 3(a) shows the angular variation of the central group. The satellites are found to be composed of pairs symmetrically located around each of the central lines and with intensity (per pair) $\approx5\%$ of the corresponding central component.

The complete spectrum can be described as arising from several identical defects, but differently oriented in the lattice, each with the spin Hamiltonian

$$\mathcal{H}=\beta\mathbf{H}\cdot\mathbf{g}\cdot\mathbf{S}+\sum_j \mathbf{I}_j\cdot[\mathbf{A}_j\cdot\mathbf{S}-(\mu_j/I_j)\mathbf{H}], \qquad (1)$$

with $S=\frac{1}{2}$.

The second term describes magnetic hyperfine interactions with nuclei neighboring the defect. In these

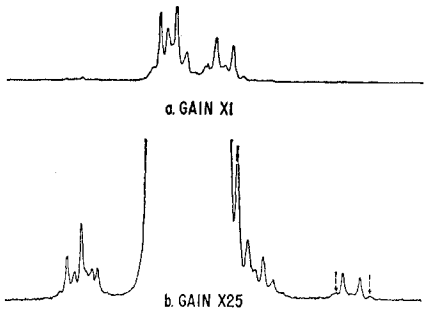

FIG. 2. E-center spectrum at two gain settings with $\mathbf{H}\|\langle111\rangle$. The arrows indicate weak shoulders on the satellite lines, which are referred to in the text.

interactions, there are two distinct nuclear species involved. One is a nucleus with a 100% abundant isotope of $I=\frac{1}{2}$. (We will demonstrate in the next section that this nucleus is that of a phosphorus atom near the defect, hence we will refer to it here as phosphorus.) There is always one and only one such phosphorus nucleus near the defect, giving rise to the doublet structure on all lines shown in Figs. 2 and 3. The other nuclear species is Si^{29} (4.7% abundant, $I=\frac{1}{2}$) associated with neighboring silicon atoms. The satellites of Fig. 2 arise from strong interaction with the Si^{29} nucleus of *one* nearby silicon atom, their amplitudes relative to the central lines reflecting the isotopic abundance of Si^{29}. Hyperfine interactions with other silicon atoms in the vicinity of the defect are an order of magnitude smaller and are only partially resolved, contributing mainly to the breadth of the central lines.

Equation (1) gives for the energy levels

$$E=g\beta HM+\sum_j E_{hf}{}^j(M,m_j)\,, \tag{2}$$

with

$$g^2=g_1{}^2n_1{}^2+g_2{}^2n_2{}^2+g_3{}^2n_3{}^2\,, \tag{3}$$

where n_1, n_2, n_3 are the direction cosines of the principal axes of the g tensor with respect to **H**. Ignoring the small anisotropy in g, the hyperfine energy terms in (2) are

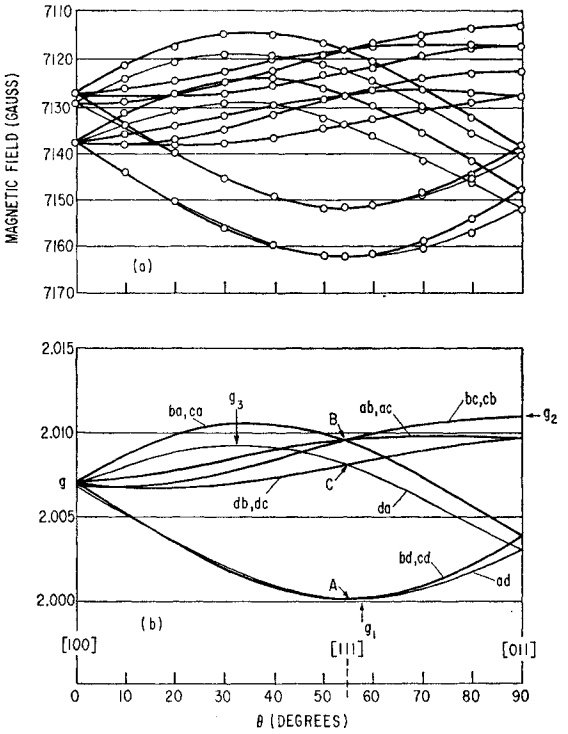

FIG. 3. (a) Angular dependence of the central lines in the E-center spectrum with **H** in the $(0\bar{1}1)$ plane (see Fig. 4). The microwave frequency was 20.029 kMc/sec. (b) Corresponding g values. The labeling scheme is described in the text.

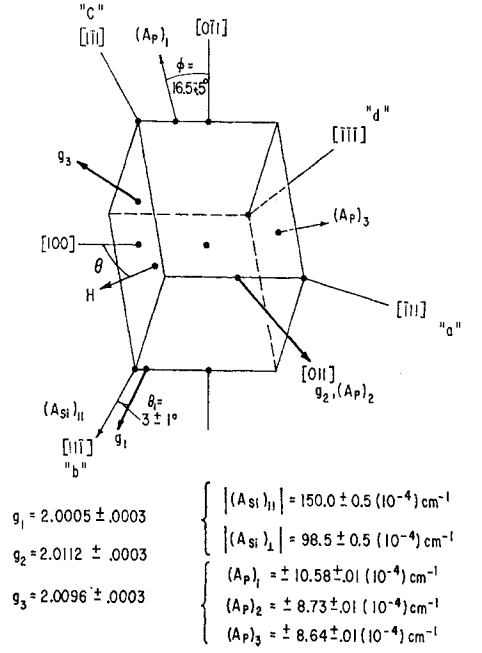

FIG. 4. Spin Hamiltonian constants for the E center with axes indicated for one of the twelve equivalent defect orientations in the lattice. With the magnetic field **H** in the $(0\bar{1}1)$ plane as shown, this set of axes gives rise to the g values given by cb in Fig. 3(b).

given to first order in $A/g\beta H$, $\mu/g\beta I$ by

$$E_{hf}{}^j(M,m_j)=\frac{M}{|M|}m_j\{\sum_\alpha [MA_{j\alpha}-(\mu_j/I_j)H]^2n_{j\alpha}{}^2\}^{1/2}. \tag{4}$$

Here $n_{j\alpha}$ are the direction cosines of the $\alpha=1$, 2, 3 principal axes of the $\mathbf{A}_j$ tensor with respect to **H**. Equation (4) has been written in a form convenient for use when $|MA_{j\alpha}|>|\mu_j/I_j|H$, the case for the hyperfine interactions studied here. In so doing, the selection rules for the allowed EPR transitions are the usual $\Delta M=\pm1$, $\Delta m_j=0$,[9] giving

$$g\beta H=h\nu_0-\sum_j [E_{hf}{}^j(\tfrac{1}{2},m_j)-E_{hf}{}^j(-\tfrac{1}{2},m_j)]. \tag{5}$$

The analysis is summarized in Fig. 4, where the principal values of the **g** and **A** tensors are given along with their principal axes for one of the possible defect orientations.[10] From Fig. 4, it is seen that there must be 24 equivalent orientations available for the defect in the cubic silicon lattice. That is, for each of the twelve possible $\langle 110\rangle$ axes for g_2, there are two equivalent

[9] If $|MA_{j\alpha}|<|\mu_j/I_j|H$, omission of the term $M/|M|$ in Eq. (5) will allow the use of the same selection rules.

[10] These values for $\mathbf{A}_P$ were determined also by ENDOR measurements to be described in the next section. They are therefore more accurate than the values determined by analysis of the doublet splitting in the EPR alone. These results are within the stated error of our previously published results (Refs. 3, 4) but reveal in addition the tilting of the $(A_P)_1$ axis by $\varphi=16.5$ deg away from $[0\bar{1}1]$, a fact not previously noted.

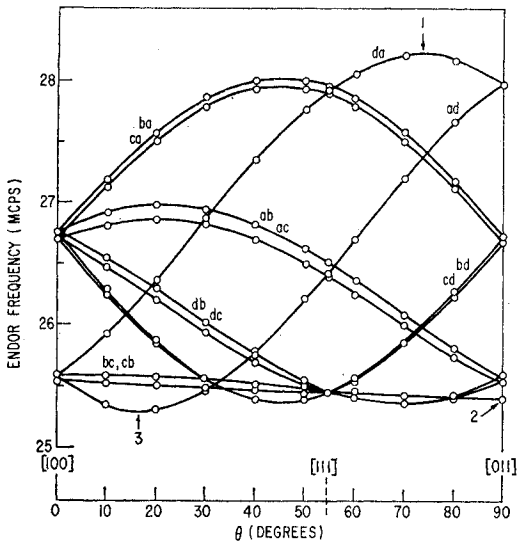

FIG. 5. Angular dependence of the P^{31} ENDOR frequencies with **H** in the (01̄1) plane. The labels denote the corresponding branches of the spectrum in Fig. 3(b) for which these transitions are observed.

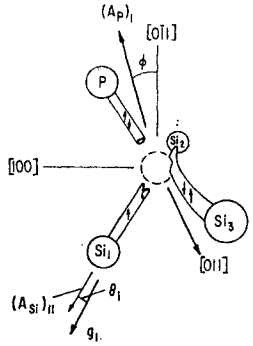

FIG. 6. Simple model of the E center as the neutral charge state of a vacancy next to a substitutional phosphorus atom.

choices for g_1, one being generated from the other by a 180-deg rotation around g_2. In the EPR spectrum, such a rotation, or inversion, of coordinates cannot be distinguished and the number of distinguishable spectra is reduced to twelve. For most of the studies described here, the spectra were studied with **H** in a {110} plane (i.e., crystal rotated around the corresponding ⟨110⟩ axis). In this case ten of the spectra become equivalent by pairs, giving only seven distinct spectra as shown in Fig. 3, five of double intensity, and two of unit intensity.

We label (for later use) the transitions of Fig. 3 as referring to a specific defect orientation. This has been done as follows: In Fig. 4, the four ⟨111⟩ axes are labeled "*a*," "*b*," "*c*," and "*d*." (We do not distinguish here the *sign* of the axis direction.) We label a defect by two letters. The first letter specifies the ⟨111⟩ axis closest to $(A_P)_I$ and the second specifies the direction of $(A_{Si})_{II}$.

3. *ENDOR Spectrum*

ENDOR studies were initiated primarily in order to identify the impurity giving rise to the 100% abundant $I=\frac{1}{2}$ hyperfine splitting.[11] From Eq. (4), the nuclear resonance frequencies ($\Delta M=0$, $\Delta m_j=\pm 1$) are

$$\nu_n{}^j(M)=\frac{1}{h}\{\sum_\alpha [MA_{j\alpha}-(\mu_j/I_j)H]^2 n_{j\alpha}{}^2\}^{1/2}. \quad (6)$$

The study was performed only on the higher frequency transition, the lower frequency transition usually being too weak to detect.

The frequencies of the ENDOR transitions versus magnetic field orientation in the {110} plane are shown in Fig. 5 for each of the branches of the spectrum shown in Fig. 3, and are labeled accordingly. Also indicated are the positions of the principal hyperfine axes as determined from these measurements. (The splitting of the *ba–ca*, *bd–cd*, *ab–ac*, *db–dc*, and *bc–cb* pairs arises from ≈1.5 deg misalignment of the ⟨110⟩ axis of the crystal around which the orientation studies were made and would not exist if the crystal were perfectly aligned.)

The $A_{j\alpha}$ can be determined from the doublet splitting in the EPR spectrum, as described in the previous section. With these, we may solve (6) for μ_j using the ENDOR frequencies of Fig. 5. The result is $|\mu_j|=1.13\pm 0.06$. Phosphorus ($\mu_P=+1.1305$[12]) is the only atom in the periodic table with a 100% abundant $I=\frac{1}{2}$ nucleus in this range and the atom involved has therefore been proven to be phosphorus.

Having identified the atom as phosphorus, we may now use the more accurate value,[13] $\mu=+1.1305$, to determine the values of $\mathbf{A}_P$ along the principal axes and these are given in Fig. 4. Also, for greater accuracy, we modify Eq. (6) to include terms second order in $A/g\beta H$. This gives for the ENDOR transition with **H** along a principal axis (α) of $\mathbf{A}_j$,

$$(h\nu_n{}^j)_\alpha=\Big|A_{j\alpha}M-(\mu_j/I_j)H-(A_{j\beta}A_{j\gamma}/2h\nu) \times[S(S+1)-M^2]-\frac{A_{j\beta}{}^2+A_{j\gamma}{}^2}{4h\nu}M(2m-1)\Big|. \quad (7)$$

Here ν is the EPR frequency, and $A_{j\beta}$ and $A_{j\gamma}$ are the other two principal values of **A**. These second-order

[11] The sensitivity, although adequate for the study of this 100% abundant nucleus, was not sufficient to study the 4.7% abundant Si^{29} hf interactions. As a result this interesting part of the problem, i.e., probing out the wave function on more distant silicon neighbors, has yet to be done.

[12] H. Kopfermann, *Nuclear Moments* (Academic Press, Inc., New York, 1958), p. 451.

[13] In assuming this value for μ, we are ignoring possible contributions to the magnetic field at the nucleus arising from the orbital angular momentum induced into the wave function by the external magnetic field—the equivalent of the "chemical shift" in NMR studies. Using arguments similar to those given by G. W. Ludwig and H. H. Woodbury [Phys. Rev. **117**, 1286 (1960)], we conclude, from the small g shifts encountered here, that the effect is negligible with respect to the experimental errors indicated in Fig. 4.

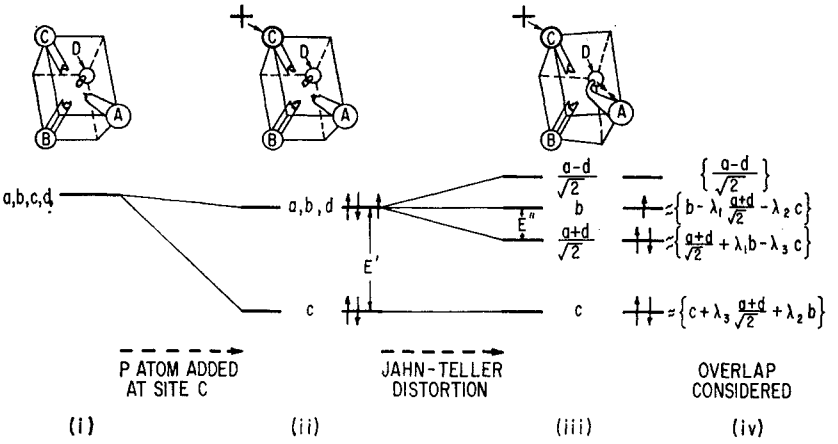

FIG. 7. Simple LCAO molecular orbital model of the electronic structure of the E center. (i) Four degenerate (ignoring overlap) orbitals of the isolated vacancy. (ii) The lowering of the c orbital due to the extra nuclear charge of the phosphorus atom at C. (iii) Lifting of the degeneracy of the a,b,d orbitals by a Jahn-Teller distortion. (iv) Modifications to the wave functions when small overlap between the atomic orbitals is considered. (These wave functions are orthogonal and normalized only through first order in the λ_i.)

corrections are small, and were therefore used only in determining the principal values given in Fig. 4. Equation (6) was otherwise quite satisfactory for fitting the observed spectra. The absolute signs of $A_{j\alpha}$ could not be determined, but fitting the data of Fig. 5 with Eq. (6) requires that the signs of all principal values be the same.

B. Discussion

1. Model

In order to interpret the experimental results, it will be convenient to present an approximate description of the model at the outset. This is shown in Fig. 6 for the defect giving rise to the specific sets of axes shown in Fig. 4. It is the neutral charge state of a lattice vacancy trapped next to a substitutional phosphorus atom impurity. We can visualize the construction of the defect as follows: Initially, there are four broken bonds around the vacancy, one each for the four atoms surrounding it. Because of the extra nuclear charge of the phosphorus atom, two electrons are accommodated in its broken orbital with their spins paired off. Two of the remaining silicon atoms pull together to form an electron pair bond leaving an unpaired electron in the orbital of the remaining silicon atom. EPR arises from this unpaired electron explaining the large hyperfine interaction with one silicon atom. The $\mathbf{A}_{Si}$ and $\mathbf{g}$ axes reflect primarily the $\langle 111\rangle$ axis of the broken bond orbital on this silicon atom.

A somewhat more detailed consideration of the electronic structure of the defect is shown in Fig. 7. In the absence of overlap, the dangling orbitals of an isolated lattice vacancy (a,b,c,d) associated with the four neighboring silicon atoms (A,B,C,D) give four degenerate one-electron orbitals. Replacing atom C by a phosphorus atom is equivalent to adding an extra positive charge at this site. This partially removes the degeneracy and orbital c is lowered in energy. In the neutral charge state, five electrons are accommodated in these orbitals, two paired in the c orbital and the remaining three in the a,b,d set. Because of the degeneracy associated with the partially filled a,b,d orbitals, a spontaneous distortion takes place to remove this degeneracy, as shown. Viewed this way, the "pair bonding" of silicon atoms 2 and 3 in Fig. 6 can be considered simply as a manifestation of the Jahn-Teller[14] effect.

If we now consider the effect of small additional overlap between the remaining orbitals, the wave functions will be modified slightly as shown in panel (iv) of Fig. 7. In this scheme, the unpaired electron is primarily located in orbital b of silicon atom B but has a small percentage $(\lambda_1^2/2)$ on silicon atoms A and D and (λ_2^2) on phosphorus atom C. Because we expect the Jahn-Teller splitting (E'') to be smaller than the Coulomb energy associated with the lowering of the c orbital (E'), we expect $\lambda_1^2>\lambda_2^2$.

This is still a considerable oversimplification, of course, because the electronic wave functions will also spill over somewhat onto the more distant neighbors. However, analysis of the hyperfine interactions in the following section shows that $\sim 70\%$ of the wave function can be accounted for on these four atoms alone and this simple localized "molecule" should therefore be a reasonable first approximation.

In the next two sections the hyperfine interactions and the g tensor will be considered quantitatively in terms of this model. In the remaining sections, other consequences of the model will be explored as quantitative tests for the model.

2. Hyperfine Interactions

Following the arguments of the previous section, let us construct the wave function for the unpaired electron as a linear combination of atomic orbitals centered on the atom sites near the defect

$$\bar{\psi}=\sum_j \eta_j\psi_j. \tag{8}$$

[14] H. A. Jahn and E. Teller, Proc. Roy. Soc. (London) **A161**, 220 (1937).

TABLE I. Hyperfine parameters (a_j and b_j) and the corresponding molecular wave function coefficients (α_j^2, β_j^2, and η_j^2) calculated from the observed hyperfine interaction constants for the atom sites in the vicinity of the E center.

Atom site	a_j (10^{-4} cm^{-1})	b_j (10^{-4} cm^{-1})	α_j^2	β_j^2	η_j^2
Si_1	(−)115.7	(−)17.2	0.14	0.86	0.59
Si_2	(−) 12.4	···	(0.30)	(0.70)	0.03
Si_3	(−) 12.4	···	(0.30)	(0.70)	0.03
P	(+) 9.32	(+) 0.63	0.29	0.71	0.01

At each atom site j, we approximate ψ_j as a hybrid $3s3p$ orbital given by

$$\psi_j=\alpha_j(\psi_{3s})_j+\beta_j(\psi_{3p})_j. \tag{9}$$

For the atoms adjacent to the vacancy, we take the p function as directed approximately along the ⟨111⟩ direction from the site to the center of the vacancy. To a good first approximation, the hyperfine interaction at the jth nuclear site is determined solely by ψ_j, i.e., that part of the wave function close to the nucleus. In this approximation, the hyperfine interaction is axially symmetric along the p-orbital axis and can be written

$$\begin{aligned} A_{\parallel}&=a+2b,\\ A_{\perp}&=a-b. \end{aligned} \tag{10}$$

Here the isotropic term a arises from the Fermi contact interaction

$$a_j=(16\pi/3)(\mu_j/I_j)\beta\alpha_j^2\eta_j^2|\psi_{3s}(0)|_j^2, \tag{11}$$

where μ_j is the magnetic moment and I_j the spin of the jth nucleus. The anisotropic term b results from the dipole-dipole interaction averaged over the electronic wave function and is given by

$$b_j=(4/5)(\mu_j/I_j)\beta\beta_j^2\eta_j^2\langle r_{3p}^{-3}\rangle_j. \tag{12}$$

In Appendix A, we have estimated $|\psi_{3s}(0)|^2$ and $\langle r_{3p}^{-3}\rangle$ for neutral silicon and phosphorus, using the recent Hartree-Fock calculations of Freeman and Watson.[15] These values are given in Table III in the Appendix.

Table I gives the results of analysis for α_j^2, β_j^2, η_j^2 for each of the atom sites of Fig. 6, using Eqs. (8)–(12), the hyperfine constants given in Fig. 4 and the estimates of Table III. Equations (11) and (12) predict that a_j and b_j should have the same sign as μ_j. With this assumption, there is no ambiguity in determining the a_j and b_j from (10) even though the absolute values of $A_{\parallel}$ and $A_{\perp}$ were not determined. The signs of the a_j's and b_j's in Table I are in parenthesis to indicate that they were not determined experimentally. In treating the phosphorus hyperfine interaction we have ignored the small departure from axial symmetry $[(A_P)_2\neq(A_P)_3]$ and have ignored the additional contribution to b_j that arises from dipole-dipole interaction with the unpaired electron centered mainly on the neighboring Si_1 site. A crude calculation suggests that this interaction contributes $\sim 0.1-0.2$ (10^{-4} cm^{-1}) to the anisotropic term and it should be included in a more sophisticated treatment. It appears small enough, however, that it cannot account by itself for the tilting of the hf axis away from the ⟨111⟩ "normal bond" direction and we must conclude that the orbital on the phosphorus is itself significantly tilted in this direction.

The estimates of a_j for the Si_2 and Si_3 sites comes indirectly from an experiment to be described in a later section (Sec. IVA), and is included here at this time for completeness. Only a_j can be estimated in this experiment and we have had to assume α_j^2 and β_j^2, i.e., percentage s and p, in order to compute η_j^2. The choice of $\alpha^2\approx 0.30$, $\beta^2\approx 0.70$ was made to agree with that observed in the A center,[16] where the unpaired electron is incorporated in a similar two atom bond between next neighbors across a vacancy.

We are thus able to account for $\sim 60\%$ of the wave function as localized in a dangling orbital on a single silicon atom (Si_1 of Fig. 6, atom B of Fig. 7) neighboring the vacancy. The orbital is approximated by $\sim 86\%$ $3p$ character and is directed toward the vacancy. The enhanced p-like character over a $25\%s-75\%p$, (sp^3), tetrahedral orbital[17] could be caused by the relaxing of the Si_1 atom away from the vacancy. Since the orbital on this atom is not involved in bonding to the other atoms across from the vacancy (see Fig. 7), we would expect the Si_1 atom to be pulled away from the vacancy by the strong bonds to its three remaining nearest neighbors (not shown in Figs. 6 and 7). Si_1 and its three nearest neighbors would then tend to approach a planar configuration for which the bonding orbitals would be sp^2 and the dangling orbital pure p.[18]

An additional $\sim 7\%$ of the wave function is accounted for on the three other atoms surrounding the vacancy, $\sim 3\%$ each on the two silicon atoms (Si_2 and Si_3) and a still smaller amount ($\sim 1\%$), as anticipated in the previous section, on the phosphorus. The remaining $\sim 30\%$ of the wave function is presumably spread over more distant silicon neighbors. [The hyperfine interaction with some of these sites is still large enough to give partially resolved structure on the shoulders of the lines in the spectra (see Fig. 2). The Si_2 and Si_3 interactions contribute to these shoulders, but the total intensity of the structure indicates that there must also

[15] R. E. Watson and A. J. Freeman, Phys. Rev. **123**, 521 (1961).

[16] Our previous analysis of the A center (Refs. 1,4) with somewhat different estimates of $|\psi_{3s}(0)|^2$ and $\langle r_{3p}^{-3}\rangle$, indicated that, for it, the wave function was 37% s and 60% p on the main two silicon atoms next to the vacancy and with 70% of the total wave function accounted for by them. A reanalysis, using the new estimates of these quantities given in Table III, gives $\sim 30\%$ s and $\sim 70\%$ p, but with essentially the same fraction of the wave function accounted for. Similar changes, in the fraction s and p character only, are required for the other centers analyzed in Ref. 4.

[17] L. Pauling, *The Nature of the Chemical Bond* (Cornell University Press, Ithaca, New York, 1948), 2nd ed., Chap. 3.

[18] The arguments are developed somewhat more fully in Ref. 4.

be three or four additional sites for which the hyperfine interaction is of comparable magnitude. These then could account for an additional 10–15% of the wave function leaving only 15–20% to be further spread out. The weaker hyperfine interaction on these more distant sites is unresolved and contributes only to the breadth (~2.5 G between half-maximum points) of the central part of the line.]

3. *g* Tensor

We have determined that the wave function consists primarily of a dangling bond on a single silicon atom. Let us therefore consider the *g* tensor to be expected for such a single broken-bond orbital. We start with the Hamiltonian for a bound electron in a magnetic field.[19]

$$\mathcal{H}=2\beta\mathbf{H}\cdot\mathbf{S}+\frac{e\hbar}{2mc}\mathbf{S}\cdot\left[\mathbf{E}\times\left(\mathbf{p}+\frac{e}{c}\mathbf{A}\right)\right]+\frac{e}{2mc}(\mathbf{p}\cdot\mathbf{A}+\mathbf{A}\cdot\mathbf{p})+\frac{e^2}{2mc^2}A^2. \quad (13)$$

The second term gives rise to the spin-orbit interaction where **E** is the electric field seen by the electron, **p**, its momentum and **A**, the vector potential. The third term gives the interaction between the motion of the electron and the external magnetic field, and the last term is the usual diamagnetic interaction.

We choose a gauge for **A** with the atom involved as center, i.e.,

$$\mathbf{A}=\tfrac{1}{2}\mathbf{H}_0\times\mathbf{r}. \quad (14)$$

With this choice, the third term becomes $\beta\mathbf{H}_0\cdot\mathbf{L}$. Equation (13) then leads to the following expression for the *g* shift, accurate to first order in the spin-orbit interaction,

$$\Delta g_{ij}=-2\sum_n \frac{\langle 0|(\mathbf{V}_{so})_i|n\rangle\langle n|L_j|0\rangle}{E_n-E_0}. \quad (15)$$

where

$$\mathbf{V}_{so}=(\beta/mc)\mathbf{E}\times\mathbf{p}.$$

The sum is over all excited states.

The form of the *g* tensor to be expected is apparent from Eq. (15). It will be axially symmetric around the direction of the broken bond orbital axis and the *g* shift along the axis will be zero.[20] There can be a nonzero *g* shift perpendicular to this axis, however.

We note that the observed *g* tensor (Fig. 4) is approximately axially symmetric around the 1 axis (which is approximately the bond axis, see Fig. 6), as expected. Also, the *g* shift along this axis, although not zero, is significantly smaller than that along the 2 and 3 axes. If we consider the small negative shift along the bond axis as arising from the 40% of the wave function *not* accounted for in this oversimplified treatment, we are left with $\Delta g_{\parallel}=0$ and $\Delta g_{\perp}\approx+0.01$ to be contributed by the dangling bond. Since ≈60% of the wave function is in this bond, this requires $\Delta g_{\parallel}=0$, $\Delta g_{\perp}\approx+0.017$ for a fully occupied dangling bond.

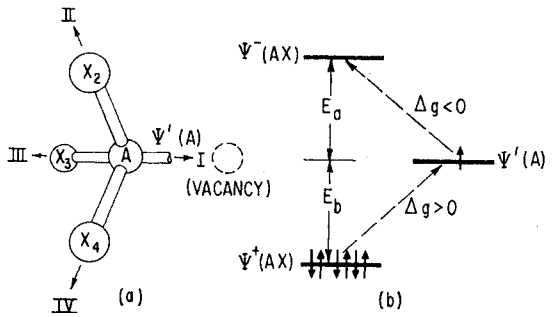

FIG. 8. Localized "molecule" considered in the *g*-shift calculation (see Appendix B). (a) Atom *A* with its broken bond $\bar{\psi}'(A)$ next to a vacancy. (b) Corresponding one-electron molecular states. The matrix elements involved in the *g* shift are indicated along with the sign of their contribution.

Experimentally, we can take the view that these values are reasonable in that other defect structures in silicon which we have studied and interpreted in terms of dangling bonds also indicate $\Delta g_{\parallel}=0$ and with positive values for $\Delta g_{\perp}$ of this magnitude.[1,4] Theoretically, however, the calculation of these quantities represents a very complex problem. Treated properly, the excited states of Eq. (15) are the continuum of all valence and conduction band states of the solid.

In previous publications,[1,4] we have carried out a simplified treatment of this problem in which we considered only the localized "molecule" made up of the atom in question and its three nearest neighbors as shown in Fig. 8. In this treatment, we used simple one-electron LCAO bonding $[\bar{\psi}^+(AX)]$ and antibonding $[\bar{\psi}^-(AX)]$ molecular orbitals between the atom and its neighbors as approximations to the excited localized valence and conduction band states of (15). The matrix elements to the bonding orbitals, being "hole"-like, were shown to give rise to a positive *g* shift, while those to the antibonding ones, being "electron"-like, gave rise to a negative shift. The net shift was shown to be the difference between these two *competing* effects. However, it has been pointed out to us that in the derivation, the spin-orbit matrix elements were not handled correctly,[21] leading to an error in the final result. We take this opportunity to correct this error. The result (rederived in Appendix B) should

[19] C. P. Slichter, *Principles of Magnetic Resonance* (Harper and Row, Publishers, Inc., New York, 1963), Chap. 7.

[20] The orbital may be made up of a linear combination of several atomic orbitals (*s*,*p*,*d*, etc.), but by symmetry, all will have $m_l=0$ along the bond axis. As a result, there are no matrix elements for the component of angular momentum along this axis giving $\Delta g_{\parallel}=0$.

[21] We are grateful to R. H. Silsbee for pointing out this error to us. Our error involved replacing $\mathbf{V}_{so}$ by $\lambda\mathbf{L}$, with λ the spin-orbit constant for the free atom. For the molecular excited states considered here, the more general form of (15) should have been used.

have been

$$\Delta g_1 \approx \lambda\{[1/E_b)-(1/E_a)\}\beta_A^2, \qquad (16)$$

where λ is the spin-orbit interaction constant for the $3p$ electron of atomic silicon, β_A^2 is the percentage $3p$ character for the dangling bond, and E_b and E_a are the energies to the bonding and antibonding orbitals, respectively, as shown in the figure. The overlap integral between the atomic orbitals on the atom and its neighbors no longer appears in the result.

In order to estimate E_b and E_a, we recognize that making up a localized state in the band picture requires summation over all k. E_a and E_b must therefore represent suitable averages over the available states in the bands. Present estimates of the band structure of silicon[22] would suggest that these average excited state energies would be $\sim$1–2 V into the respective bands from the band edges. We do not know the energy-level position associated with the dangling bond of the E center but we *do* know that an *additional* electron can be accommodated at $(E_c-0.4)$eV. This means that the single electron level is lower in energy and, as a guess, we take it as $\approx E_v$, the valence band edge. This gives $E_b \approx 1.5$ eV, $E_a \approx 2.5$ eV. With $\lambda=0.02$ eV,[23] $\beta_A^2=0.86$ (Table I), this gives

$$\Delta g_1 \approx +0.005.$$

This is the correct sign but is a factor of $\sim$3 too low. There was some arbitrariness in the estimates of E_b and E_a, to be sure, but it is not felt that a realistic adjustment of the values could make up this large a factor. (This is particularly evident in the Si-A center,[1] for instance, where the energy level is known to be close to the *conduction band* edge and the g shifts are still positive and of comparable magnitude.)

We thus conclude that the large g shifts must result, in significant part, as a result of stronger matrix elements of (15) to the bonding orbitals (valence band) than to the antibonding ones (conduction band). Within the framework of our localized molecule approximation, there are two effects that we did not previously treat that tend in this direction. One results from the fact that the molecular obritals used in (I) were not orthogonal to the $1s$, $2s$, $2p$ atom cores. We have modified the treatment to take this properly into account (see Appendix B) and we find that (16) is replaced by

$$\Delta g_1 \approx \lambda\{(1+\gamma)/E_b-(1-\gamma)/E_a\}\beta_A^2. \qquad (17)$$

In Appendix B, we estimate $\gamma\sim+0.17$, giving, with $E_b \approx 1.5$ eV, $E_a \approx 2.5$ eV,

$$\Delta g_1 \approx +0.008.$$

This is an increase in the right direction but it is still not enough.

Another effect is a *nuclear shielding* effect. The effect of the positive charge of the neighboring atom core should be to enhance the charge density near the core of the atom to which it is bound for the bonding orbitals but to deplete it for the antibonding ones. This effect is well established in the H_2 molecule, for instance, where the contraction of the $1s$ atomic orbitals in the bonding state is equivalent to an increase of nuclear charge by 20%.[24] Such a contraction in our case would enhance the spin-orbit matrix element of (15) and further increase the "contact" to the valence band.

It would be difficult to include this effect properly in our simple LCAO treatment. However, a measure of its importance is seen in the fact that the observed spin-orbit splitting in the valence band of silicon (0.044 eV)[25] is actually $\sim$50% *greater* than that for the free atom, (0.03 eV).[23] On the other hand, if we were to calculate the spin-orbit splitting using the LCAO molecular bonding orbitals in (I), we would get a *reduction*. For instance, if we ignore the $2p$ core terms, the effective spin-orbit constant would be reduced directly by the normalization factor $(1+S)\cong 1.7$ [see (I)]. By a calculation similar to that for the g shift, we find that inclusion of the $2p$ core terms recovers some of this loss by the factor $1+2\gamma=1.34$, but we would still predict a reduction of $\sim$1.25. This would indicate that the "contraction" of the valence band wave functions is therefore of considerable importance.

It is interesting to note that in our simple treatment, it would require an effective $\gamma\sim 0.8$, to account for the observed 50% increase in valence band spin-orbit interaction. Such a value in (17) would give $\Delta g_1 \approx +0.017$! This agreement is clearly not entirely coincidental in that both the g shift and the enhanced valence band spin-orbit interaction reflect the same phenomenon—the contraction of the wave function around the cores in bonding states.[26]

We conclude that the indicated values $\Delta g_{11}=0$, $\Delta g_1 \approx +0.017$ are *reasonable* ones for a single broken bond orbital in silicon. In the case of the E center, with $\sim$60% of the wave function in such an orbital, this accounts for the gross features of the g tensor, i.e., $\Delta g_1 \approx 0$, $\Delta g_2 \approx \Delta g_2 + 0.01$. The remainder of the wave

[22] J. C. Phillips, Phys. Rev. **125**, 1931 (1962).

[23] The spin-orbit interaction constant λ is two-thirds the free atom spin-orbit splitting as given in C. E. Moore, *Atomic Energy Levels*, Natl. Bur. Std. (U. S.) Circular No. 467 (U. S. Government Printing Office, Washington, D. C., 1949).

[24] See C. A. Coulson, Trans. Faraday Soc. **33**, 1479 (1937) for a discussion of these effects.

[25] S. Zwerdling, K. J. Button, B. Lax, and L. M. Roth, Phys. Rev. Letters **4**, 173 (1960).

[26] The correct characterization of molecular wave functions in the vicinity of the atomic cores is a subject of considerable current controversy [W. Marshall and R. Stuart, Phys. Rev. **123**, 2048 (1961); R. G. Shulman and S. Sugano, *ibid.* **130**, 506 (1963); J. C. Phillips and L. Liu, Phys. Rev. Letters, **8**, 94 (1962)]. In the case of substantial ionic character, the situation is not so clear. In the case here of strong covalent bonds, however, it appears that substantial contraction and expansion of the bonding and antibonding orbitals, respectively, must occur around the atoms. The article by Phillips and Liu, and Ref. 54 treat this point in some detail.

function (~40%) presumably can account for the remaining g shifts.

IV. MOTIONAL EFFECTS

In the previous sections, we have presented a model for the E center, and we have shown that it is compatible with the observed hyperfine interaction and the g tensor. There is always the question, however, as to whether this model is unique. Are there other possible microscopic configurations that might also be compatible with these quantities? We desire to test the validity of the model in as many ways as possible.

The model of Fig. 6 predicts a number of motional effects which we will test in the following sections. For instance, for the particular phosphorus-vacancy direction shown in the figure, there are two other entirely equivalent configurations, corresponding to bonding Si_1 and Si_3 together and leaving the unpaired electron on Si_2, or Si_1 and Si_2 together, with the unpaired electron on Si_3. These together with the configuration depicted in Fig. 6, represent the three equivalent Jahn-Teller distortions of Fig. 7. The barrier for reorientation from one distortion direction to another should not be large (being comparable to the Jahn-Teller energy) and we expect thermally activated reorientation to manifest itself at relatively low temperatures. This motion can be studied in the resonance in two ways: (1) If the correlation time for the reorientation process is short enough ($\tau \lesssim 10^{-7}$ sec), the individual lines in the EPR spectrum become lifetime broadened and give a direct means of studying the nature and kinetics of the motion. Such a study is described in Sec. IVA; (2) in IVB, the motion is revealed by studying the preferential alignment of the defects induced by the application of uniaxial stress to the crystal. In addition to revealing the nature and kinetics of the reorientation process, the magnitude and sense of the stress induced alignment also confirm other important features of the model.

The vacancy-phosphorus direction is another "degree of freedom" that can be probed by stress. In Sec. IVC, preferential alignment of this axis of the defect is achieved by stress at elevated temperatures. The study of the magnitude and sign of the alignment plus the kinetics of its recovery gives a further test of the model.

A. Low-Temperature Linewidth Studies

In the temperature region ~60–150°K, the E center spectrum is observed to change drastically as shown in Fig. 9.[27] Initially, some of the lines appear to broaden and disappear as the temperature is raised and at the higher temperature end a simplified spectrum emerges.

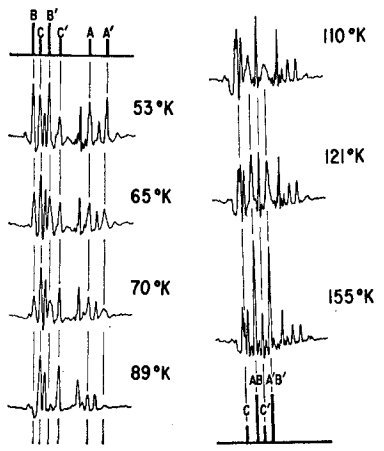

FIG. 9. E-center spectrum versus temperature showing the effect of thermally activated reorientation from one Jahn-Teller distortion direction to another (Ref. 27), $\mathbf{H} \| \langle 111 \rangle$.

This behavior suggests thermally activated reorientation of the defects. In general, if a defect with an anisotropic g tensor is jumping from one orientation in the lattice to another, its g value will change abruptly with each orientation. In the resonance experiment, this means that, if we are tuned to a particular multiplet in the spectrum (which corresponds to the g value of a particular orientation for the defect), a given defect is alternately brought into resonance, then out, as it executes this random reorientation. This will give rise to a lifetime broadening of the multiplets. As the temperature is raised and the jumping rate increases, the multiplets will tend to broaden out and disappear. At higher temperatures and higher jump rates, motional narrowing will eventually begin and new sets of lines will emerge at the average position of the original multiplets.

Now let us consider the E center in detail and, in particular, determine what we expect if the reorientation motion is from one Jahn-Teller distortion to another. Figure 3(b) shows the variation of the g value versus crystalline orientation for the differently oriented defects. By reference to Figs. 4 and 6, we recognize that the labels on the various curves of Fig. 3(b) have a simple interpretation in terms of the model for the defect. Labeling the four different $\langle 111 \rangle$ axes a through d as in Fig. 4, the first letter of the label specifies the vacancy-phosphorus direction and the second letter specifies the direction from the vacancy to the silicon atom with the unpaired electron. Stated more simply, *for the nearest neighbor sites of the vacancy depicted in Fig. 7, the first letter of the designation gives the phosphorus site and the second letter gives the silicon site for the unpaired electron.* (The defect orientation of Fig. 6 is "*cb*.")

Now consider the thermally activated reorientation from one Jahn-Teller distortion direction to another. In terms of the defect labeling scheme, each time a defect executes a reorientation, its second letter changes,

[27] Also noticed in Fig. 9. are weaker lines, not associated with the E center, which do not change throughout this temperature region. Some of these arise from another center which appears to have roughly the same g variations as the E center and which also displays a phosphorous hyperfine splitting, but of approximately half the magnitude. The interference with the E-center spectrum, and its weaker intensity, has prevented a detailed analysis. We have no model for this defect but presumably it could be an E center paired off with another defect such as oxygen or another vacancy, etc.

but its first does not. The corresponding g-value change can be read directly from Fig. 3(b).

We now treat the particular case when the magnetic field is parallel to a ⟨111⟩ axis (the conditions of Fig. 9). Referring to Fig. 3(b), the number of distinguishable g values reduces to three, labeled A, B, and C. With the phosphorus hyperfine interaction, this gives rise to three *pairs* of lines for the central group spectrum as shown in Fig. 3(a) and as designated in Fig. 9 as A, A', B, B', and C, C'. Consider now that the magnetic field is tuned to resonance for multiplet C (or C'). For the defects giving rise to this multiplet, the particular reorientation we are considering has no effect because each of the three Jahn-Teller distortions gives rise to the identical g value. (This multiplet arises from the defects for which the magnetic field is pointing along the phosphorus-vacancy direction. By symmetry, it is apparent that each of the three distortions is equivalent with respect to this axis.) Therefore the motion predicts no effect on the CC' multiplets. (There will be a slight narrowing due to the partial motional averaging of Si^{29} hf broadening by neighbors, but we ignore this in this discussion.) In Fig. 9, it is noted that these multiplets (C' is easiest to observe) do indeed stay sharp throughout this temperature range in agreement with the predictions.

The defects with the other three phosphorus-vacancy directions give rise to resonance at $A(A')$ or $B(B')$ and, for them, reorientation causes a jumping between the two resonance values. Gutowsky and Saika[28] have treated a problem which is formally similar to this and we can apply their results directly to this problem. Their results are shown schematically in Fig. 10, in which we consider hopping between two resonance fields A and B separated by $\delta\omega=(g\beta/\hbar)\Delta H$, and with relative probabilities p_A and p_B of being at each of these two fields. (For our case $p_A=\frac{1}{3}$, $p_B=\frac{2}{3}$.) At low temperatures, we have two lines (I) of relative amplitudes p_A and p_B and with widths determined by static interactions (in our case, Si^{29} hf interactions with distant neighbors). As the characteristic reorientation time τ becomes shorter (II), the motion contributes a Lorentzian broadening

$$g(\omega)=\frac{(T_2/\pi)}{1+(\omega_0-\omega)^2T_2^2} \tag{18}$$

to each of the multiplets, where T_2 for each multiplet is given in the figure. At higher temperatures where $\tau\delta\omega\ll 1$, (III), motional narrowing is manifested by the emergence of a line at the weighted average between A and B, which is again Lorentzian broadened with the $(T_2)_{AB}$ given in the figure. As τ becomes shorter the central line narrows further ultimately going over into a temperature-independent width now determined by static interactions that have not been averaged out.

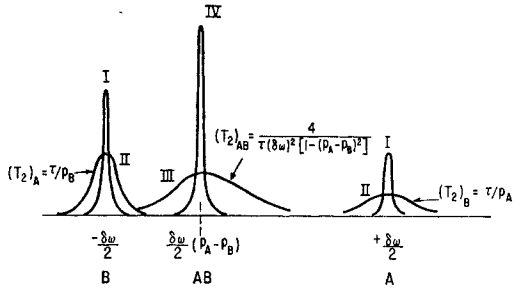

FIG. 10. Effect of thermally activated "hopping" between two resonance positions A and B, with relative probabilities p_A and p_B of being at each site, according to Gutowsky and Saika (Ref. 28). As the temperature increases and the lifetime τ for the "hopping" process decreases, the spectrum changes from (I) low-temperature multiplets at A and B, to (II) broadening of multiplets, to (III) disappearance of multiplets and emergence of a line at the average position AB, to (IV) narrowing of the averaged line.

[28] H. S. Gutowsky and A. Saika, J. Chem. Phys. **21**, 1688 (1953). The formulas in Fig. 10 are derived from Eq. (18) of this reference.

Inspection of Fig. 9 shows that the AA' and BB' multiplets broaden as predicted (A' and B show clearly the broadening and final disappearance in the first panel with A' twice the width of B as expected throughout), along with the ultimate emergence and narrowing of the $AB-A'B'$ pair at the weighted average position in the second panel. Similar studies with $\mathbf{H}\|\langle 100\rangle$ and $\mathbf{H}\|\langle 110\rangle$, also confirm the expectations of the model. The motionally averaged spectrum at elevated temperature is axially symmetric reflecting the phosphorus-vacancy direction around which the averaging has taken place. The g values within experimental accuracy agree with those predicted from the weighted averages of the values in Fig. 3(b).

Using the formulas for T_2 in Fig. 10, we can estimate τ from a study of the linewidths versus temperature in both the early broadening and final narrowing regions. The results are given in Fig. 11. {In measurement, the linewidths $\Delta\omega=(g\beta/\hbar)\Delta H$ were taken as the width between half-maximum points observed in the derivative of dispersion recordings as in Fig. 9. For a line of Lorentzian shape, $T_2=1/\Delta\omega$. The points plotted at each temperature represent the *average* of two different methods for subtracting out the contribution due to the static width, $(\Delta\omega)_0$. One method assumed $T_2=[\Delta\omega-(\Delta\omega)_0]^{-1}$, the result expected for the convolution of two Lorentzian shapes. The other took $T_2=[\Delta\omega^2-(\Delta\omega)_0^2]^{-1/2}$, somewhat characteristic of two Gaussians. Since we anticipate the correct behavior to be somewhere in between these two simple approaches, we have simply averaged the two estimates. The accuracy of the data (limited by overlapping of lines, presence of unrelated spectra, temperature uncertainties, etc.) does not warrant a more detailed treatment. We recognize also that a detailed treatment is not trivial. For instance, the static contributions are not strictly constant, being themselves presumably partially motionally narrowed throughout the same region.}

In spite of the uncertainties, we could make a

reasonably good estimate of τ because the broadening and narrowing regions are separated by about two decades. However, we will defer this until the next section, where additional experimental data allow a more accurate estimate. We note only that the activation energy is $\sim$0.06 eV.

Study of motional effects on the Si^{29} satellites is also informative. This is shown in Fig. 12 for $\mathbf{H}\|\langle 100\rangle$. At 20°K, (observed under fast passage conditions in dispersion), we see the Si^{29} satellites with a total splitting of 126 G. In the motionally averaged state (displayed in the figure as derivative of absorption, explaining the apparent difference in the character of the resonance), the Si^{29} satellites are found to be $\approx$ three times as intense relative to the central group but with a splitting reduced to 51 G. This is just what we expect because in the motionally averaged state, the defect becomes a *three* silicon center. That is, in the model of Fig. 6, the unpaired electron is hopping between the Si_1, Si_2, and Si_3 sites so fast as to be indistinguishable from a defect in which the electron is in a LCAO molecular orbital spread over all three. The hyperfine satellites now arise when any one of the three equivalent silicon sites is Si^{29}, which is three times as probable as one, and therefore three times as intense. The hyperfine splitting is determined now by

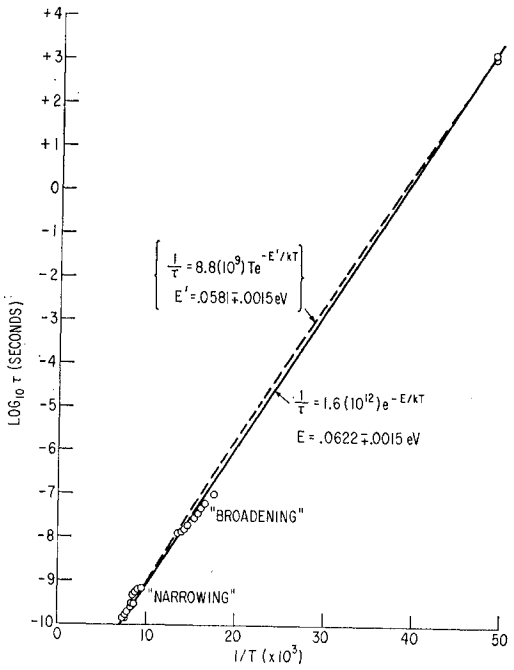

FIG. 11. Lifetime τ of the Jahn-Teller reorientation versus temperature. The two curves represent fits to two different theories (see text).

$$A'(\langle 100\rangle)=\tfrac{1}{3}A_1(\langle 100\rangle)+\tfrac{1}{3}A_2(\langle 100\rangle)+\tfrac{1}{3}A_3(\langle 100\rangle), \quad (19)$$

where $A_1(\langle 100\rangle)$ is the hf term for the defect configuration of Fig. 6 when Si_1 is Si^{29}, and A_2 and A_3 are the correspondingly smaller terms when Si_2 and Si_3 are Si^{29}. The meaning of Eq. (19) is that if one of the three silicon sites is a Si^{29} there is an interaction of A_1 for the third of the time the electron is located mostly on that atom but there is also A_2 and A_3 for each of the other one-thirds when the electron is primarily located on the other two silicon atoms.

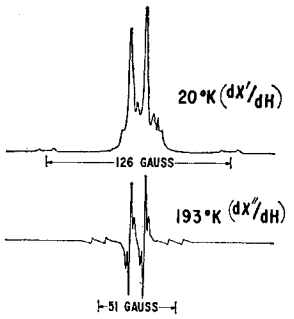

FIG. 12. Comparison of the motionally averaged E-center spectrum at 193°K with that at 20.4°K at $\mathbf{H}\|\langle 100\rangle$.

With $|A'(\langle 100\rangle)|=51$ G, $|A_1(\langle 100\rangle)|=126$ G, we can solve Eq. (19) for A_2 and A_3, which must be equal by symmetry. This gives

$$A_{2,3}(\langle 100\rangle)=\pm 13.2 \text{ G}=\pm 12.4(10^{-4})\text{cm}^{-1},$$

where the sign must be the same as $A_1(\langle 100\rangle)$. Assuming the interaction to be axially symmetric along a $\langle 111\rangle$ direction, this gives the isotropic constants a_2 and a_3 which are entered in Table I.

Summary: Forgetting the model for a moment, we have determined the following about the center as a result of the linewidth studies: The center undergoes thermally activated reorientation around a particular $\langle 111\rangle$ axis associated with the defect. The activation energy is low ($\sim$0.06 eV), and from the hyperfine studies we have determined that the motion is an *electronic* one. That is, this is *not* the reorientation of a molecular unit but is rather an electronic *bond switching* in which the unpaired electron hops between *three* equivalent atoms which are for all purposes fixed in the lattice.

In terms of the model, this is precisely the behavior expected for thermally activated reorientation of the defect from one Jahn-Teller distortion direction to the other. The 0.06 eV we feel is a reasonably value for the activation energy of the process.[29] This must be considered an important confirmation of the model.

B. Low-Temperature Stress Studies

All of the possible orientations of the E center are equally probable in the cubic silicon lattice and, at

[29] In a simple model, the three silicon atoms go through the symmetrical undistorted position in reorienting. In this case, the 0.06 eV would be equal to the Jahn-Teller stabilization energy. Remembering that this energy is the difference between the total electronic stabilization energy and the increased energy stored in the lattice, which in turn is half the electronic energy, we get for the electronic stabilization energy 0.12 eV. In Fig. 8, this energy is associated with two electrons in the $(a+d)$ orbital so that the energy per electron $E''\approx 0.06$ eV.

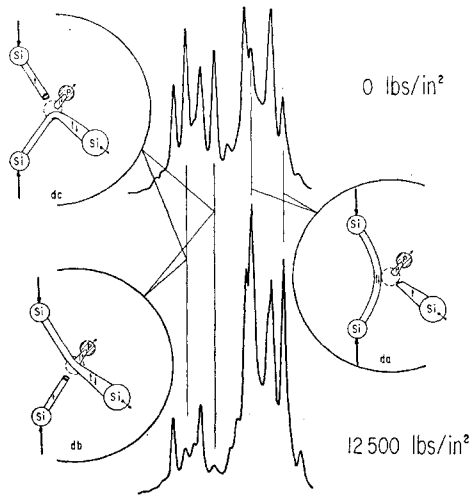

FIG. 13. Change in the E-center spectrum (H‖[011]), under [01$\bar{1}$] compressional stress. The insets show a typical defect orientation for each multiplet.

thermodynamical equilibrium, we have equal numbers of defects in each of these orientations. If we now strain the crystal, and distort it from cubic symmetry, the various orientations are no longer equivalent and, if the defects are free to reorient, they will do so, tending to seek out the lowest energy orientation. This stress induced alignment is the static analog of the internal friction experiment.

EPR gives a unique way of observing the alignment in that the amplitudes of the multiplets in the spectrum give a direct measure of the relative number of defects in each of the allowed orientations, allowing a microscopic study of the process.[30] We here apply this to study the same "bond-switching" motion that was described in the previous section.

In Fig. 13, the effects on the spectrum of applying a uniaxial compressional stress along a ⟨110⟩ axis of the crystal at 20.4°K is observed. (The spectrum is observed with the magnetic field along another ⟨110⟩ axis, perpendicular to the stress direction.) The insets identify a representative set of defects—and their corresponding letter designation—to be associated with each multiplet. It is seen that there is a large effect, the *dc* and *db* orientations being strongly suppressed and the *da* being proportionally enhanced. This is again consistent with the "bond-switching" motion, the phosphorus-vacancy direction remaining unchanged. (The intensity simply "sloshes" between the indicated multiplets with no change in total area.) The *sense* of the alignment is an *additional* confirmation of the model in that the defect prefers to align in such a way that the applied compression serves to push the two bonding silicon atoms closer together as expected. In terms of Fig. 7, the applied stress adds to the Jahn-Teller distortion and lowers the electronic energy of the defect. We will return to the magnitude of the alignment but first let us consider the kinetics.

Upon removing the stress at 20.4°K, the recovery to the original unstressed spectrum is observed to follow a single exponential law with a time constant $\tau=1.3\pm0.2(10^3)$ sec. This τ is the same characteristic reorientation time that appears in the formulas of Fig. 10 for the linewidth studies and is therefore also plotted in Fig. 11. This value together with the linewidth study estimates span 13 decades in τ, allowing a very accurate determination of τ. The points fall well on a straight line giving

$$\tau^{-1}=1.6(10^{12})e^{-E/kT}, \tag{20}$$

with $E=0.0622\pm0.0015$ eV. [There is some disagreement in the literature as to whether (20) is the correct form for such a process or whether T should appear in the pre-exponential factor.[31] For this reason, we have also shown by the dashed line the best fit with the alternate form. We do not feel our data are accurate enough in their present state to distinguish between the two although the fit using Eq. (20) appears somewhat better. We point this out because with these large ranges of τ and $1/T$, our experimental errors in the estimated activation energies become less than that imposed by the uncertainty in the theory. It is possible that a careful study in this or similar systems[32] could serve as a critical test of the two theories.]

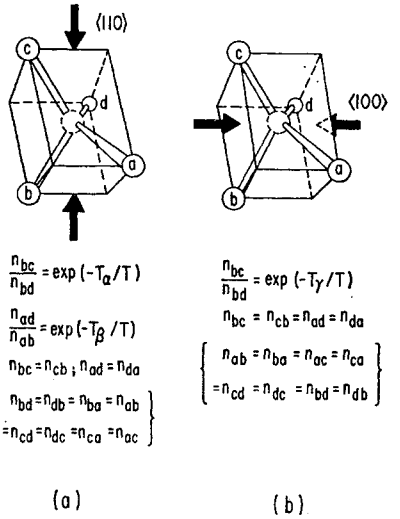

FIG. 14. Boltzmann factors governing the populations of the different defect orientations for the (a) ⟨110⟩ and (b) ⟨100⟩ stress experiments. The subscripts *ij* refer to the defect orientation according to the convention established in the text.

[30] A detailed study of another EPR center (the Si-*A* center) using this technique has been previously described by us in (I). See also W. Kanzig, Phys. Chem. Solids **23**, 479 (1962).

[31] See R. H. Doremus, J. Chem. Phys. **34**, 2186 (1961) for a discussion of this point and for further references to the literature.

[32] The silicon divacancy [G. D. Watkins and J. W. Corbett (to be published)] also has two spectra which are suitable for such a study.

A quantitative study of the *degree* of alignment has also been performed versus stress and temperature. For this, the effects of stress along both ⟨100⟩ and ⟨110⟩ axes were investigated. By symmetry, the ⟨100⟩ stress creates two nonequivalent sets of orientations while the ⟨110⟩ stress creates three (see Fig. 14). Assuming a Boltzmann distribution between the sets, this defines a single energy difference kT_γ for the ⟨100⟩ stress and two, kT_α and kT_β, for the ⟨110⟩ stress as indicated in the figure.

Fit to a Boltzmann distribution given by the formulas in Fig. 14, the alignment in all cases shows T_α, T_β, and T_γ linearly proportional to stress within experimental accuracy. The exponential dependence upon $1/T$ has also been verified. For this study, estimates in the range 20–50°K were made from the relative intensities of the multiplets as described above. An estimate was also made at 160°K from the *shift* in the resonance field of the motionally averaged spectrum (reflecting the relative change of p_A and p_B in Fig. 10). The fact that *shifts* in the *positions* of the resonance multiplets at high temperatures occur, and that they can be accurately predicted by measurements on the relative *amplitudes* of the multiplets in the low-temperature spectrum confirms again that the high-temperature phase is properly characterized as a motional averaging of the low-temperature configurations.

In Table II, the measured values for T_α, T_β, and T_γ determined at a stress of 12 360 lb/in.^{2} are given. To interpret these, let us take a very simple view of the defect. We assume that the change in energy of a particular defect orientation is determined solely by the component of strain along the line joining the two bonding silicon atoms (Si_2 and Si_3 of Fig. 6).

We define a change in the defect energy per unit strain along this direction as

$$M=(dE/d\epsilon)_{\mathrm{Si-Si}}. \tag{21}$$

Defining ϵ_{ad} as the strain along the line joining the *ad* sites, etc., we obtain

$$\begin{aligned} kT_\alpha&=(\epsilon_{ad}-\epsilon_{ac})M\,,\\ kT_\beta&=(\epsilon_{bc}-\epsilon_{cd})M\,,\\ kT_\gamma&=(\epsilon_{ad}-\epsilon_{ac})M\,. \end{aligned} \tag{22}$$

These follow directly from the formulas of Fig. 14 when the change in energy of the *bc* site is set equal to $M\epsilon_{ad}$, etc. In (I) these strains have been calculated in terms of the elastic moduli and applied stress and, using these formulas with Eq. (22), we can solve for M using the experimental values of Table II. Selection of M for the best fit gives

$$M=+16.8 \text{ eV/unit strain.}^{33} \tag{23}$$

[33] In footnote 29, we concluded that the electronic stabilization energy associated with the Jahn-Teller distortion was ~0.12 eV. This, with Eq. (23) serves to define an "effective" strain associated with the Jahn-Teller distortion of ~0.7%. Whether this in turn bears any simple relation to the actual motions of the atoms neighboring the vacancy is not clear, however.

TABLE II. Comparison of the observed and calculated (see text) energy differences (in °K) for the differently oriented defects under stress (see Fig. 14). The applied stress is 12 360 psi.

Stress	T_j	Observed (°K)	Calculated (°K)
⟨110⟩	T_α	+ 9	+11
	T_β	−90	−94
⟨100⟩	T_γ	+85	+81

The values computed from Eq. (22) using this constant are also given in Table II.

The agreement in Table II is quite good considering the oversimplified model that we have taken in the analysis. The positive value of M means that the energy is lowered when the atoms are pushed together as we would expect for two normally next nearest neighbors with rather weaker overlap. The magnitude of M is close to the value +16.0 eV/unit strain deduced in (I) for a similar Si-Si pair bond in the A center. As in the A center, we argue that the magnitude is not unreasonable being of the same order of magnitude as deformation potentials in silicon.[34] We thus conclude that the stress experiments give substantial additional confirmation to the model.

C. High-Temperature Stress Studies

There is another "degree of freedom" for the defect, the phosphorus-vacancy axis, which has not been probed as yet. In the low-temperature studies this axis remained fixed. In terms of the model, it should be more difficult for this axis to change because *atoms* must rearrange rather than the easier *electronic* rearrangement involved in the low-temperature motion.

This phosphorus-vacancy axis reorientation can be revealed by stress alignment at elevated temperatures. For this a crystal was compressed along a ⟨110⟩ axis to ~26 000 psi at room temperature in an external squeezing apparatus for ~1 h, then removed and quickly inserted into the microwave cavity and cooled to 20.4°K for study. A significant alignment was achieved as can be seen in Fig. 15. By reference to Figs. 3(b) and 14, we see that the preferred direction for the phosphorus-vacancy axis is in the plane perpendicular to the stress direction.

From Fig. 15, we estimate the degree of alignment[35]

$$\frac{n_\perp}{n_\parallel}=\frac{n_{ad}+n_{ac}+n_{ab}}{n_{bc}+n_{ba}+n_{bd}}\cong 1.75. \tag{24}$$

Analysis of Eq. (24), similar to that in the previous section where we consider only the $M=16.8$ eV/unit

[34] C. Herring and E. Vogt, Phys. Rev. **101**, 944 (1956).

[35] We estimate the alignment in Fig. 15 to be 1.5. We increase this value by ~15% to take account of partial recovery during the ~75 sec at room temperature between removal of stress and eventual cooling of the sample (see Fig. 16).

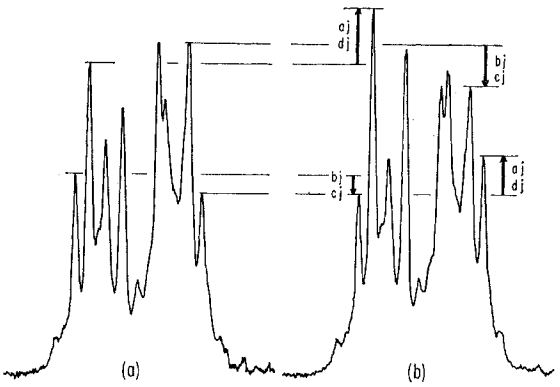

FIG. 15. E-center spectrum (**H**$\|[011]$) (a) before and (b) after 26 000 psi $[0\bar{1}1]$ compressional stress at room temperature. The defect orientations corresponding to the lines in the spectrum are indicated.

strain associated with the Si–Si bond, predicts $(n_\perp/n_{\parallel})=1.34$. The alignment is therefore in the same sense as that dictated by the preference of the defect to align its Si–Si bond along the compressed direction. If we include another parameter for the change in energy per unit strain at right angles to this, along the phosphorus-vacancy direction,

$$N=(dE/d\epsilon)_{\text{P–Vac}}\cong -9 \text{ eV/unit strain}, \quad (25)$$

the value of 1.75 is obtained. The sign is consistent with an outward relaxation of the phosphorus atom from the vacancy in its normal configuration which is to be expected since there is no bonding to hold it in (see Fig. 7). It is not possible to make a value judgment on the magnitude, but it does not seem out of line with the value for M, for instance.

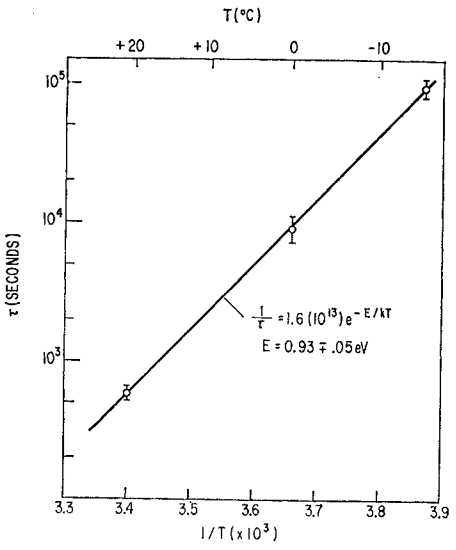

FIG. 16. Characteristic recovery time versus temperature for the phosphorous-vacancy axis reorientation.

The kinetics of the reorientation process was studied by monitoring the recovery from the stress induced alignment versus annealing. During each anneal, the sample remained in the cavity which in turn was held at the annealing temperature for a specified time interval. At the end of each annealing interval, the cavity was plunged back into the cryostat and the remaining alignment monitored from the spectrum at 20.4°K. The results are shown in Fig. 16. We obtain for the characteristic relaxation time of the reorietnation process,

$$\tau^{-1}=1.6(10^{13})\exp(-E/kT),$$

with

$$E=0.93\pm 0.05 \text{ eV}.$$

Let us now inquire as to the microscopic process by which the defect reorients. That is, of what process are we measuring the kinetics? Interchange of the phosphorus and vacancy serves only to "invert" the defect and does not achieve the reorientation we are observing. The most likely remaining process is the one shown in Fig. 17 in which the vacancy must make four consecutive jumps, two away from the phosphorus and then two back. The fact that the defect must partially disassociate in order to reorient has some interesting consequences.

First let us note that the combination of reorientation plus the phosphorus-vacancy interchange allows the defect to diffuse through the lattice as an entity. We anticipate the activation energy for the vacancy-phosphorus interchange to be small, being comparable to the value for the isolated vacancy motion ($\sim\frac{1}{3}$ eV).[36] The limiting process for diffusion should therefore be the reorientation. We thus conclude that in measuring the activation energy for reorientation, *we are also measuring the activation energy for the diffusion of the phosphorus-vacancy pair in the lattice.*

The fact that the vacancy must separate partially from the phosphorus in order for the defect to reorient gives a simple explanation as to why the activation energy is larger than that associated with the isolated vacancy motion. The difference ($\sim$0.6 eV) can be associated with binding energy that must be overcome in order for the vacancy to separate to the next-next-nearest neighbor position (position 3 in Fig. 17). This is not the *total* binding energy, however, because we do not detect any loss in E centers in the process. That is, there is still sufficient binding at this remote position to assure that most of the vacancies return.

There are several bits of experimental information that give us guides in estimating the remaining binding energy at this next-next-nearest site. For instance, we note that the E centers decay upon standing at room temperature at a rate suggestive of a time constant $\lesssim$6 weeks.[37] On the other hand, from Fig. 16, we deter-

[36] G. D. Watkins, J. Phys. Soc. Japan **18**, Suppl. II, 22 (1963).

[37] The actual rate may be slower than this. The loss of E centers in the spectrum can also be caused by decay of other centers which in turn alters the Fermi level so that E centers still present are no

mine that the defect is reorienting once every ~400 sec at this temperature (~25°C). We may therefore conclude that the vacancy gets away only once in $\gtrsim 10^4$ opportunities at the next-next-nearest site. This, in turn, can be related to a Boltzmann factor weighting the separation and recapture processes at this site,

$$\alpha \exp(-\Delta E/kT) \lesssim 10^{-14}, \tag{26}$$

where α is a geometric factor (~1). Taking $\alpha=1$, we obtain $\Delta E \gtrsim 0.25$ eV. This quantity is not strictly equal to the binding energy at this site but rather gives a difference in barrier heights as shown in Fig. 18. However, it is clearly related (being perhaps somewhat larger) and serves as an indication of its magnitude.

It is interesting to note that a calculation of the binding energy between a single positive and a single negative charge separated by the same distance and immersed in a dielectric constant equal to that of silicon (11.6) gives 0.28 eV. This is certainly suggestive

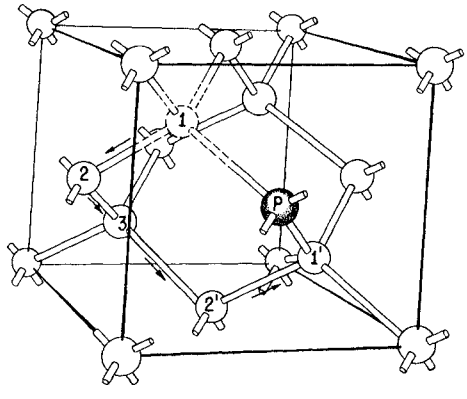

FIG. 17. The mechanism for the phosphorus-vacancy axis reorientation. The vacancy in the normal nearest position (No. 1) must make two jumps away from the phosphorus to site No. 3 and then return to a new (No. 1′) nearest site.

and perhaps not an unreasonable way to view the defect at this separation. The over-all defect is neutral and, in separating into components, the phosphorus will tend to be positively charged, its normal ionized state when isolated.

The indication that $\gtrsim 10^4$ reorientations are occurring before disassociation means that the defect is diffusing through the lattice as an entity for considerable distances. Considering the approximate nature of these estimates it is not clear then whether the annealing of the E center actually is a result of its dissociation or whether it is the result of long-range migration as an entity with subsequent trapping by other defects. An experiment that may bear upon this is that reported by Saito *et al.*[38] They have studied by electrical measure-

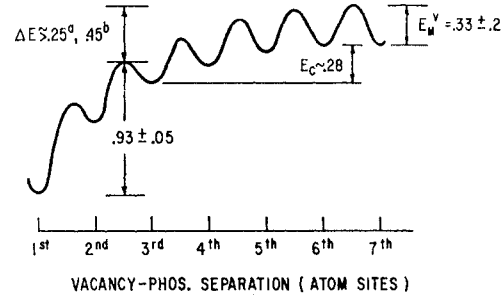

FIG. 18. The potential energy (in eV) of a vacancy in the vicinity of a substitutional phosphorus atom, as determined from the experiments on the E center. The abscissa denotes the various neighbor positions in order of increasing separation, and are not necessarily in a straight line. The quantity ΔE was estimated from annealing studies by (a) EPR and (b) electrical measurements.

ments the annealing kinetics of a deep acceptor at $(E_c-0.4)$eV in floating zone silicon produced by irradiation. Considering the conditions of their experiment, it is possible that they are monitoring the E center anneal, as they have suggested. They observe first-order kinetics with a characteristic recovery time τ given by[39]

$$\tau^{-1} \cong 10^8 \exp(-0.94/kT).$$

The close agreement of this activation energy to that which we estimate for *diffusion* suggests that the annealing they are studying is the diffusion to traps. This is also consistent with the pre-exponential factor of 10^8 indicating, with our pre-exponential factor of $\sim 10^{13}$ for the single reorientation process, $\sim 10^5$ diffusional jumps before trapping. Analysis similar to that leading to (26), but using $\gtrsim 10^5$ jumps without separation and at the higher temperatures of anneal used by Saito *et al.* (~175°C) gives $\Delta E \gtrsim 0.45$ eV. This value is also indicated in Fig. 18.

On the other hand, there is also evidence for dissociation in that some Si-A centers (oxygen-vacancy pairs) are observed to form as the Si-E centers disappear. This has been observed in electrical measurements[40] and has also been observed by us in resonance. These vacancies could be liberated of course, after trapping. In any event, we recognize from our estimates here that it is touch and go as to whether the vacancy and phosphorus stay together long enough to reach a trap as an entity or whether they dissociate first, and that probably both processes are occurring. To investigate this in detail one would require studies over a wide range of temperatures and defect concentrations.

V. SUMMARY AND CONCLUSIONS

We conclude that the Si-E center resonance arises from the neutral charge state of a lattice vacancy ad-

longer in the proper charge state for resonance. This complication has discouraged us from making detailed annealing studies for this center.

[38] H. Saito, M. Hirata, and T. Horiuchi, J. Phys. Soc. Japan **18**, Suppl. III, 246 (1963).

[39] We have estimated the pre-exponential factor from the curves of Fig. 6 of their paper. (See Ref. 38.)

[40] G. K. Wertheim and D. N. E. Buchanan, J. Appl. Phys. **30**, 1232 (1959).

jacent to a substitutional phosphorus atom. It is presumably formed when a lattice vacancy, formed at random in the lattice by irradiation, diffuses through the lattice, and is trapped by the phosphorus impurity. It appears to be the dominant defect formed in phosphorus-doped floating zone silicon by electron irradiation at room temperature. In pulled crystals, containing oxygen $\sim 10^{17}-10^{18}$ cm^{-3}, this center is not observed, the oxygen now serving as the dominant vacancy trap to form the Si-A center.[1] The Si-E center introduces an acceptor level at $\sim(E_c-0.4)$eV. With the Fermi level position above this level, the defect is negatively charged and is not observed in the resonance.

The model of the center deduced from the studies in this paper is one in which two of the three silicon atoms adjacent to the vacancy pull together to form a pair bond with the unpaired electron observed in the resonance left primarily to the third silicon atom. This distortion can be viewed as a manifestation of the Jahn–Teller effect. The primary confirming features in the spin resonance are summarized as follows:

(1) Analysis of the resolved Si^{29} hyperfine interactions indicates that $\sim 60\%$ of the wave function is localized in a dangling bond on a single silicon atom. An additional 20–25% of the wave function can be accounted for by partially resolved hyperfine interactions on a few (5-6) near-neighbor sites, with the remaining 15–20% presumably spread out over more distant sites.

(2) The spectrum also reveals resolved hyperfine interaction with a 100% abundant $I=\frac{1}{2}$ impurity. ENDOR measurements confirm that this impurity is phosphorus. Only $\sim 1\%$ of the wave function is localized on this atom.

(3) The g tensor is nearly axially symmetric reflecting the axis of the dangling bond which makes up most of the wave function. Its anisotropy is similar to other defects which we have studied and have identified as made up of dangling bonds associated with vacancies. Also, a simple "localized molecule" treatment of the defect has been given which indicates that the magnitude and sign of the g shifts are reasonable.

(4) Motional broadening and narrowing effects are observed in the spectrum in the temperature region 60–150°K and are attributed to the thermally activated reorientation from one Jahn-Teller distortion direction to the other. Analysis confirms that the motion is that of an electronic "bond switching" (not atom motion) and that the motion is around the phosphorus-vacancy axis as predicted by the model.

(5) This motion is also studied by stress induced alignment at 20.4°K. Combined with the linewidth studies, the kinetics of the reorientation process can be obtained with very high precision. The observed activation energy ~ 0.06 eV appears reasonable for this process. The *sense* of the alignment is consistent with the natural preference of the defect to align so that the applied stress aids the Jahn-Teller distortion. The *degree* of alignment can be accounted for by a simple model which only considers the change in energy per unit strain along the axis joining the bonding Si-Si pair. The magnitude deduced for this parameter is reasonable, being of the order of observed deformation potentials.

(6) Stress-induced alignment of the phosphorus-vacancy axis is also studied. The sense and magnitude can also be accounted for in terms of the model. The kinetics of this process, with an activation energy of 0.93 ± 0.05 eV, appear reasonable for the atom rearrangements required by the model.

The E center, in addition to being an important defect in radiation damage studies, may play an important role in unirradiated silicon. High-temperature diffusion of substitutional impurity atoms, as well as self-diffusion, is generally believed to be via lattice vacancies. As a result, such impurity-vacancy interactions are important in understanding the mechanics of impurity diffusion. The E center represents a unique opportunity to probe this interaction in detail. Being the neutral charge state appropriate for the Fermi level in the middle of the gap, it is in the correct charge state relevant to the high-temperature experiments. In Fig. 18, we summarize what we have been able to learn about this interaction. The abscissa denotes schematically the different neighboring atom positions as one moves out from the phosphorus. They are not necessarily in a straight line. We don't know the exact shape to be expected but it seems reasonable to assume it is something as shown. From the kinetics of the stress-orientation of the phosphorus-vacancy axis we have determined the height of the second maximum to be 0.93 ± 0.05 eV, as indicated. We have also made two estimates for the indicated difference in barrier heights ΔE from annealing studies. The smaller estimate comes from EPR measurements and the larger one comes from electrical measurements. From previous studies[36] we estimate that the activation energy for the isolated vacancy motion is[41] $E_M{}^V=0.33\pm0.20$ eV. The indicated estimate of the binding energy $E_C\sim 0.28$ eV at the third-neighbor site comes from a simple calculation of the electrostatic interaction between a negative vacancy at this site and a positive phosphorus atom. This value is seen to be generally consistent with the other experimentally determined estimates.

We have therefore been able to deduce quite a bit about the details of the phosphorus-vacancy interaction. It is hoped that future experiments can narrow further

[41] The value for p-type silicon has been determined to be (Ref. 36) 0.33 ± 0.03 eV. However, in annealing studies in n-type silicon (Refs. 3, 36), it is found that both A and E centers emerge in two discrete temperature regions. One of these is presumably to be associated with long-range motion of the vacancy, and, depending upon which we select, we either deduce $\sim 0.1-0.2$ eV or $\sim 0.4-0.5$ eV for the activation energy of the vacancy motion. This difference from the p-type value presumably reflects the role of charge state in the mobility of the vacancy. Since we do not know the charge state appropriate to Fig. 18, we indicate an error ± 0.2 eV to bracket these extremes.

the errors in $E_M{}^V$ and ΔE with the result that this interaction will eventually be rather precisely mapped out. However, even with the present uncertainties we can draw certain conclusions:

From Fig. 18, we see that there is a sizeable binding energy ($\sim$1.0 eV) between the phosphorus atom and a vacancy in their closest bound state.[42] Because of this attractive interaction there is an enhanced probability of finding a vacancy near the phosphorus at elevated temperatures and we therefore expect the diffusion of the phosphorus to be enhanced over that for silicon self-diffusion. However, we recognize that *it is only the binding at the third-atom site that is operative in enhancing the diffusion* because the vacancy must go through this site in order for the phosphorus atom to diffuse.[43] For this binding energy, we take the Coulomb estimate E_C=0.28 eV. We estimate the error in this quantity somewhat arbitrarily as $\pm$0.15 eV, which we feel, in view of the general consistency of the values in Fig. 18, is overly cautious.

Phosphorus diffusion in silicon has been measured and the activation energy has been determined to be[44] 3.66$\pm$0.18 eV. However, there has been no corresponding measurement of self-diffusion in silicon. Using the value 0.28$\pm$0.15 eV for the lowering of the phosphorus activation energy, we therefore estimate the activation energy for silicon self-diffusion

$$E_{\text{self-diff.}}=3.94\pm0.33 \text{ eV}. \quad (27)$$

Since this quantity has not been measured directly, we feel that this probably represents the best present estimate that can be made for this important quantity.

Combining this with the activation energy for vacancy motion of 0.33$\pm$0.20 eV, we obtain for the formation energy of the lattice vacancy[45]

$$W=3.6\pm0.5 \text{ eV}. \quad (28)$$

ACKNOWLEDGMENTS

It is a pleasure to acknowledge the assistance of W. Colliton in all phases of the measurements. Helpful conversations with Dr. F. Ham, Dr. B. Segall, Dr. R. W. Redington, and Dr. R. M. Walker are also gratefully acknowledged.

APPENDIX A: ESTIMATE OF $|\psi_{3s}(0)|^2$ AND $\langle r_{3p}{}^{-3}\rangle$ FOR THE NEUTRAL $3p$ ATOMS

In previous publications,[1,4] we have used $|\psi_{3s}(0)|^2_{\text{Si}} \approx 24(10^{24})$ cm^{-3} and $\langle r_{3p}{}^{-3}\rangle_{\text{Si}} \approx 17(10^{24})$ cm^{-3} in the analysis of resonance centers. These estimates were originally made using various Hartree functions, available only for higher ionization states of silicon, as guides. Since then, Hartree-Fock calculations for neutral silicon, as well as all of the other neutral $3p$ atoms, have been reported by Watson and Freeman[15] and a revised estimate of these quantities is in order.

In Table III, the first two columns show $|\psi_{3s}(0)|^2$ and $\langle r_{3p}{}^{-3}\rangle$ determined from the Watson and Freeman wave functions[46] for the atoms aluminum through chlorine. Consider first $|\psi_{3s}(0)|^2$. As was pointed out by Kohn and Luttinger,[47] direct comparison with experiment in the case of the alkalies shows that Hartree-Fock wave functions generally underestimate $|\psi_s(0)|^2$, and the true values will probably be somewhat larger than these values. In the case of silicon, Kohn and Luttinger estimated an appropriate scaling factor by comparing the Hartree-Fock estimate of $|\psi_{3s}(0)|^2$ for the alkali-like Si^{3+} ion[48] with that predicted by the Goudsmit formula[49] for such ions and assuming the same scaling factor to apply for Si^0. Their result was that the Hartree-Fock value should be increased by $\sim$19%. Applying the same correction to the Watson and Freeman value for Si^0, we obtain the final estimate of 31.5(10^{24}) cm^{-3} shown in the table.

Now consider $\langle r_{3p}{}^{-3}\rangle$. Barnes and Smith[50] have estimated this quantity from an analysis of optical fine structure splittings and their values are given in column three of Table III for each of the $3p$ atoms. In the case of aluminum[51] and chlorine,[52] atomic beam hyperfine measurements give accurate determinations of $\langle r_{3p}{}^{-3}\rangle$, also shown in the table, to which we can compare the estimates of Barnes and Smith. We see that the agreement is very good, the atomic beam values lying $\sim$3% higher. We thus increase the Barnes and Smith estimates by 3% for the remaining atoms to give the final estimate of $\langle r_{3p}{}^{-3}\rangle$ shown in the last column.

We note that the $\langle r_{3p}{}^{-3}\rangle$ determined from the Watson and Freeman wave functions are uniformly too low. It is interesting to note that for Si^0, the value must be increased by 19% to agree with our final estimate. Although this agreement with the scaling factor for

[42] We remind the reader that these arguments (and the values in Fig. 18) apply only to the neutral charge state of the defect and therefore when the Fermi level is near the middle of the gap. This should apply to the high temperatures used in diffusion studies for anything but the most heavily doped materials.

[43] This important fact (see Sec. IVC and Fig. 17) has been generally overlooked by previous authors.

[44] C. S. Fuller and J. A. Ditzenberger, J. Appl. Phys. **27**, 544 (1956).

[45] We have, of course, assumed throughout this discussion that both phosphorus and self-diffusion proceed by the vacancy mechanism. If other mechanisms are also involved, the formation energy will be even larger.

[46] We are indebted to B. Segall for supplying us with tabulated values of the $3p$ Watson and Freeman wave functions from which $\langle r_{3p}{}^{-3}\rangle$ were calculated.

[47] W. Kohn and J. M. Luttinger, Phys. Rev. **97**, 883 (1961).

[48] W. Hartree, D. R. Hartree, and M. F. Manning, Phys. Rev. **60**, 857 (1941).

[49] S. Goudsmit, Phys. Rev. **43**, 636 (1933).

[50] R. G. Barnes and W. V. Smith, Phys. Rev. **93**, 95 (1954).

[51] H. Lew and G. Wessel, Phys. Rev. **90**, 1 (1953).

[52] V. Jaccarino and J. G. King, Phys. Rev. **83**, 471 (1951); J. G. King and V. Jaccarino, *ibid.* **84**, 852 (1951). $\langle r_{3p}{}^{-3}\rangle$ was determined from their results by analysis similar to that in the preceding Ref. 51.

TABLE III. Various estimates of $|\psi_{3s}(0)|^2$ and $\langle r_{3p}^{-3}\rangle$ for the neutral $3p$ atoms. The indicated values were determined from (HF) Hartree-Fock wave functions, (FS) experimental fine structure constants, and (AB) atomic-beam hyperfine measurements. See text for the method of determining the final estimates.

Atom	$\lvert\psi_{3s}(0)\rvert^2_{\mathrm{HF}}$ (10^{24} cm^{-3})	$\langle r_{3p}^{-3}\rangle_{\mathrm{HF}}$ (10^{24} cm^{-3})	$\langle r_{3p}^{-3}\rangle_{\mathrm{FS}}$ (10^{24} cm^{-3})	$\langle r_{3p}^{-3}\rangle_{\mathrm{AB}}$ (10^{24} cm^{-3})	$\lvert\psi_{3s}(0)\rvert^2$ Scaling factor	Final Estimates $\lvert\psi_{3s}(0)\rvert^2$ (10^{24} cm^{-3})	Final Estimates $\langle r_{3p}^{-3}\rangle$ (10^{24} cm^{-3})
Al	15.8[a]	6.94[a]	8.64[b]	8.95[c]	1.29	**20.4**	**8.95**
Si	26.4[a]	13.5[a]	15.6[b]	···	1.19	**31.5**	**16.1**
P	37.8[a]	22.0[a]	23.5[b]	···	1.10	**41.6**	**24.2**
S	53.3[a]	31.9[a]	33.9[b]	···	1.09	**58.4**	**34.9**
Cl	71.8[a]	44.2[a]	48.3[b]	49.5[d]	1.12	**80.4**	**49.5**

[a] Calculated from wavefunctions in R. E. Watson and A. J. Freeman, Phys. Rev. **123**, 521 (1961).
[b] R. G. Barnes and W. V. Smith, Phys. Rev. **93**, 95 (1954).
[c] H. Lew and G. Wessel, Phys. Rev. **90**, 1 (1953).
[d] V. Jaccarino and J. G. King, Phys. Rev. **83**, 471 (1951); J. G. King and V. Jaccarino, *ibid.* **84**, 852 (1951).

$|\psi_{3s}(0)|^2$ must be considered somewhat fortuitous, it does suggest that both $\langle r_{3p}^{-3}\rangle$ and $|\psi_{3s}(0)|^2$ are underestimated by a comparable amount in these Hartree-Fock wave functions. This then suggests a consistent way to determine the proper $|\psi_{3s}(0)|^2$ scaling factor for the other atoms: For the atoms other than Si, the scaling factor was determined as being equal to the ratio of our final estimate of $\langle r_{3p}^{-3}\rangle$ to that determined from the Freeman-Watson wave functions. The scaling factor thus determined is shown in Table III along with the corresponding final estimate of $|\psi_{3s}(0)|^2$ for all the $3p$ neutral atoms.[53]

We will not attempt to set limits of accuracy on the values of Table III. There are still sufficient uncertainties in the applicability of these free atom values to those of a bonded atom surrounding a defect in a solid to make such speculations somewhat academic for our use, anyway. However, Table III does give a set of reasonable values, consistently arrived at, for the complete $3p$ series of neutral atoms.

In this paper we have used only the values for silicon and phosphorus. In subsequent papers in this series, we will have occasion to use the estimates for others of the atoms in the table.

APPENDIX B: APPROXIMATE LCAO TREATMENT OF THE g SHIFT

We approximate the one-electron LCAO molecular orbitals of Fig. 8 as:

$$\bar{\psi}'(A)=\sigma_3{}^{I}(A)=\alpha_I\psi_{3s}(A)+\beta_I\psi_{3pI}(A),$$
$$\bar{\psi}^{\pm}(AX_2)=N^{\pm}[\sigma_3{}^{II}(A)\pm\sigma_3{}^{-II}(X_2) \mp\sum_i \epsilon_i\{\psi_i(A)\pm\psi_i(X_2)\}], \quad \text{(B1)}$$

with similar expressions for the other orbitals. Here $\sigma_3{}^{I}$, $\sigma_3{}^{II}$, $\sigma_3{}^{III}$, and $\sigma_3{}^{IV}$ represent four orthogonal cylindrical orbitals made up of $3s$-$3p$ atomic wave functions, where the superscript represents the axis of the directed orbital as shown in Fig. 8. (By $\sigma_3{}^{-II}$, we denote an orbital pointed in the opposite direction from $\sigma_3{}^{II}$.) We have included small admixtures of the core wave functions ψ_i, ($1s$, $2s$, and $2p$), in order to orthogonalize the total wave function to the core. The small admixture coefficients are given by

$$\epsilon_i=\langle\sigma_3{}^{-II}(X_2)\,|\,\psi_i(A)\rangle, \quad \text{etc.}$$

The normalization coefficients are

$$N^{\pm}=[2(1\pm S-\sum_i \epsilon_i{}^2)]^{-1/2},$$

with

$$S=\langle\sigma_3{}^{II}(A)\,|\,\sigma_3{}^{-II}(X_2)\rangle.$$

A typical orbital angular momentum matrix element of (15) is

$$\langle\bar{\psi}^{\pm}(AX_2)\,|\,L_j\,|\,\bar{\psi}'(A)\rangle = \sum_k \langle\bar{\psi}^{\pm}(AX_2)\,|\,\sigma_3{}^{k}(A)\rangle\langle\sigma_3{}^{k}(A)\,|\,L_j\,|\,\sigma_3{}^{I}(A)\rangle.$$

Substituting the expression for $\bar{\psi}^{\pm}(AX_2)$ given by Eq. (B1), and using the fact that only $\sigma_3{}^{II}(A)$ has significant overlap with any of the terms for $\bar{\psi}^{\pm}(AX_2)$, we obtain

$$\langle\bar{\psi}^{\pm}(AX)_2\,|\,L_j\,|\,\bar{\psi}'(A)\cong\tfrac{1}{2}(N^{\pm})^{-1}\langle\sigma^{II}(A)\,|\,L_j\,|\,\sigma^{I}(A)\rangle. \quad \text{(B2)}$$

Now consider the corresponding matrix element in (15) involving $\mathbf{V}_{so}$

$$\langle\bar{\psi}'(A)\,|\,(\mathbf{V}_{so})_i\,|\,\bar{\psi}^{\pm}(AX_2)\rangle = (\beta/mc)\langle\sigma_3{}^{I}(A)\,|\,(\mathbf{E}\times\mathbf{p})_i\,|\,\bar{\psi}^{\pm}(AX_2)\rangle. \quad \text{(B3)}$$

The electric field $\mathbf{E}$ is large only near the nuclei of atoms A and X_2 and therefore, in these matrix elements, tends to weight strongly only the parts of the wave functions near the atomic cores. To a good approximation we may therefore retain in Eq. (B1) only the atomic terms centered on atom A giving

$$\cong(\beta/mc)N^{\pm}\langle\sigma_3{}^{I}(A)\,|\,(\mathbf{E}\times\mathbf{p})_i\,|\,\sigma_3{}^{II}(A)-\epsilon_{2p}\psi_{2pII}(A)\rangle.$$

[53] The scaling factor is not constant throughout the series but is largest at the beginning. A further check that this variation is not unreasonable is given by noting that an even larger scaling factor of 1.42 is required in the case of neutral sodium (which starts this row in the periodic table), in order to raise the value determined from the Hartree-Fock calculations [D. R. Hartree and W. Hartree, Proc. Roy Soc. (London) **A193**, 299 (1948)] (3.56×10^{24} cm^{-3}) to that observed experimentally [P. Kusch and H. Taub, Phys. Rev. **75**, 1477 (1949)] (5.05×10^{24} cm^{-3}).

(The terms centered on atom X_2, though not zero near atom A, are slowly varying there, and therefore do not contribute significantly to the spin-orbit interaction.) Having reduced the matrix elements to those on atom A only, we may now make the substitution $\mathbf{E}=[\mathbf{r}/r]E(r)$ for the central force field near the nucleus of atom A, leading to the familiar free atom expressions

$$\langle nlm|(\mathbf{V}_{so})_i|n'l'm'\rangle=\delta_{ll'}\lambda_{nl,n'l}\langle lm|L_i|lm'\rangle,$$

with

$$\lambda_{nl,n'l}=(\beta/mc)\langle nl|[E(r)/r]|n'l\rangle.$$

This gives, upon straightforward manipulation,

$$\langle\bar{\psi}'(A)|(\mathbf{V}_{so})_i|\bar{\psi}^{\pm}(AX_2)\rangle \cong N^{\pm}[\lambda_{3p}\mp(\epsilon_{2p}\lambda_{2p,3p})/\beta_I]\langle\sigma^{\mathrm{I}}(A)|\mathbf{L}_i|\sigma^{\mathrm{II}}(A)\rangle. \quad \text{(B3')}$$

Substituting (B2) and (B3') into (15), and summing over-all excited orbitals in (B1),

$$\Delta g_{\mathrm{II}}=0,$$

$$\Delta g_{\mathrm{I}}\cong\lambda_{3p}\beta_I^2\left[\frac{1+\gamma}{E_b}\quad\frac{1-\gamma}{E_a}\right], \quad \text{(B4)}$$

with

$$\gamma=-\frac{\lambda_{2p,3p}\epsilon_{2p}}{\lambda_{3p}\beta_I}. \quad \text{(B5)}$$

Here, γ is a positive number because $\lambda_{2p,3p}$ and ϵ_{2p} will always be of opposite sign, a consequence of the fact that ψ_{3p} has one more radial node than ψ_{2p}. [In our previous treatment (I), the core overlap terms were not included in the wave functions. For these wave functions, $\gamma=0$, and (B4) leads to Eq. (16) in the text of the present paper.]

We may estimate γ, as follows: We approximate $\lambda_{2p,3p}$ as $-(\lambda_{2p}\lambda_{3p})^{1/2}$ using the values $\lambda_{2p}=0.40$ eV estimated by Liu[54] from x-ray emission data[55] and $\lambda_{3p}=0.02$ eV.[23] We calculate ϵ_{2p} from Eq. (19) using Slater atomic orbitals[56] and standard overlap integral formulas[57] in conjunction with certain required integrals tabulated by Rosen.[58] For the normal Si-Si lattice distance and with the $\sigma^i(A)$ taken as the tetrahedral sp^3 hybrids (25% $3s$, 75% $3p$), we obtain $\epsilon_{2p}=0.033$. With $\beta_I=(3)^{1/2}/2$ for the tetrahedral hybrid, this gives $\gamma\cong 0.17$.

---

[54] L. Liu, Phys. Rev. **126**, 1317 (1962).
[55] D. H. Tombulian and W. M. Cadis, Phys. Rev. **59**, 422 (1944).
[56] J. C. Slater, Phys. Rev. **36**, 57 (1930).
[57] R. S. Mulliken, C. A. Rieke, D. Orloff, and H. Orloff, J. Chem. Phys. **17**, 1248 (1949).
[58] N. Rosen, Phys. Rev. **38**, 255 (1931).